RESEARCH ARTICLE

WILEY

Effects of bonding on the performance of optical fiber strain sensors

Ignazio Floris[1,2] | Valentino Sangiorgio[1,3] | José M. Adam[1] 🄸 |
Giuseppina Uva[3] | Monica Rapido[3] | Pedro A. Calderón[1] | Javier Madrigal[2]

[1]ICITECH, Universitat Politècnica de València, Valencia, Spain

[2]iTEAM, Universitat Politècnica de València, Valencia, Spain

[3]DICATECH, Politecnico di Bari, Bari, Italy

Correspondence
José M. Adam, ICITECH, Universitat Politècnica de València, Camino de Vera s/n, 46022 Valencia, Spain.
Email: joadmar@upv.es

Summary

The structural health monitoring (SHM) of existing buildings, structures, and infrastructures has become increasingly important in recent years, while the interest of the scientific community is focused on the use of new high-performance technologies. Fiber optic sensors have become particularly attractive, thanks to their potential for monitoring strain in smart structures. The performance of this new technology depends to a large extent on the bonding technique used for its manufacture. Although the related literature has identified a correlation between some efficiency issues and the geometrical parameters of the bonding and mechanical properties of the materials adopted, the phenomenon is still not completely understood. This paper describes an in-depth study of the geometrical and mechanical parameters that influence the efficiency of optical fiber point sensors' surface bonding by synergistically related techniques such as computational simulation, experimental tests, sensor manufacturing, and data analysis. The paper's novelty is fourfold: (1) the investigation of the strain transfer mechanism of surface-bonded fiber optic sensors by considering, for the first time, all the parameters influencing the phenomenon through a considerable number of finite element (FE) analyses (117 three-dimensional FE models); (2) the development of a series of bonding efficiency predictive models; (3) the design of a specific laboratory test to validate the computational outcomes; and (4) the definition of useful guidelines for effective bonding manufacturing in order to maximize the performance of these sensors when acquiring monitoring data.

KEYWORDS

distributed sensing, fiber Bragg grating, optical fiber sensor, strain sensing, strain transfer mechanism, structural health monitoring

1 | INTRODUCTION

Most existing civil infrastructures have now exceeded their expected useful life, and their conditions have gravely deteriorated due to aging, exposure to aggressive environmental agents, and extreme weather events. To cite an instance, the American Society of Civil Engineers reported in 2017 that 39% of the bridges in the United States were more than 50 years old and 9.1% were structurally deficient, while the cost of their rehabilitation was estimated to be $123 billion.[1] The same report claimed that many dams were also in extremely serious conditions, since their average age was 56 years, while 17% were identified as potentially highly dangerous, and an investment of nearly $45 billion would be necessary for their repair. Some recent catastrophic bridge collapses (e.g., Morandi Bridge, Genoa, Italy, 2018; Mississippi Bridge, Minneapolis, Minnesota, 2007; and Kinzua Bridge, State Park, Pennsylvania, 2003) have aroused the concern of the scientific and technical community. These events underline the urgent need for effective structural health monitoring (SHM) systems.

The approaches of SHM can be principally classified according to five typologies in relation with the used methodology, technology, and accuracy of acquired information[2]: (i) vision of superficial damage,[3,4] (ii) user-based reporting,[5–8] (iii) subsurface damage detection,[2,9] (iv) dynamic parameter sensors,[10] and (v) strain measurements that is the principle feature considered for structural monitoring. Indeed, strain information helps to understand structural behavior and the possible causes of damage, such as static or dynamic loads and temperature. Many types of sensor systems are thus designed to estimate this parameter. Strain sensors can be embedded into structural elements,[11,12] but this can lead to a series of complications, including the need for miniaturization, inspectionability, maintainability, and repairability and the need to guarantee sensor operability during the operational life of the structure. On the other hand, the surface-bonding solution appears less problematic[13] and the only adoptable technique when dealing with existing buildings or structures. The two main types of strain sensors are electrical and optical.

Electrical strain sensors are a consolidated technology for nondestructive testing and evaluation and SHM.[14–16] However, in recent years, there has been an impressive development of optical fiber sensors (OFSs) by reason of their advantages over traditional sensors, such as immunity to electromagnetic interference, flexibility, lightweight, high sensitivity and accuracy, intrinsic safety, multiplexing capabilities, resistance to radiation and corrosion,[17–19] and high-speed data acquisition.[20] These innovative sensors have been applied to sense a number of different measurands, such as strain,[21] stress,[22] temperature,[23,24] moisture, vibration, slope,[25] chemicals,[26] and even curvature[27–30] and shape.[31–35] Nevertheless, strain and temperature sensors are the most widely employed technologies for SHM applications.[36,37]

To work as a strain sensor, the optical fiber is integrated with the host material (or support) and deforms together with it,[38] in most cases by means of bonding. Regrettably, OFSs oftentimes underestimate the strain of the host material due to the limited strain transfer effectiveness of their bonding and, hence, require to be rectified. Several studies have been conducted on this topic, for example, Her and Huang investigated the influence of coating stiffness and bonded length on strain transfer to OFSs by using finite element method (FEM) and performing an experimental study based on the Mach–Zehnder interferometric technique.[39] Barrias et al. carried out an experimental campaign to assess the performance of different adhesives in bonding distributed OFSs (DOFSs) on concrete surfaces, taking into account different spatial resolutions of the DOFSs.[40] Wan et al. studied the influence of different geometric bonding parameters on strain transfer by FEM.[41] Li et al. proposed a theoretical approach to calculate the strain transfer formula, considering the thickness of coating and adhesive.[42] In all the previous approaches, the parameters that influence bonding efficiency in strain transfer were only partly analyzed and, since OFSs are extensively used in SHM applications, come the necessity to thoroughly study this phenomenon.

This paper reports on an analytical and experimental study carried out to fully evaluate the strain transfer mechanism of bonded optical fiber point sensors. Its novelty consists of (1) an extensive sequence of 117 three-dimensional finite element analyses (FEAs) to study the influence of numerous parameters, including bonding length, bonding width, lower and upper thickness of the adhesive, presence of coating, and mechanical properties of the materials on bonding strain transfer performance; (2) the design of a quasi-static tensile test to evaluate the performance of distinct bonding configurations and corroborate the FEAs' outcomes by using fiber Bragg grating (FBG) sensors, the most widely used fiber optic technology for sensing applications; (3) the calibration of a series of predictive models to determine the mathematical relationships between the considered parameters and the strain transfer efficiency of surface-attached OFSs; and (4) the definition of practical and simple guide lines for correct bonding manufacture.

To summarize, this work fully defines the role of all the variables that influence the efficiency of surface-bonded fiber optic strain sensor well beyond the current state of the art. In addition, although the present study investigates the strain transfer of point sensors, in particular FBGs, many of the results here obtained, such as the effects of coating, materials stiffness, and adhesive thickness, also apply to distributed sensors. Furthermore, this research provides useful prediction models and practical guidelines that can help both the research community and industry to maximize the bonding performance.

2 | FBG SENSORS

FBGs are the most widely used OFSs and, by virtue of their high sensitivity to strain and temperature, find application in a multitude of engineering areas.[11,20,24,35,36] The foremost reasons behind this widespread use are the low cost, the large sensing length that can reach kilometers, the ability to perform dynamic sensing thanks to the high frequency data acquisition ($\sim$kHz), and the high strain sensing accuracy ($\sim$1 με).

FBGs are single-point sensors manufactured by permanently increasing the refractive index of the core of an optical fiber through its exposure to an intense laser light with a periodic pattern. This fixed refractive index modulation is a grating and has a period that is a function of the exposure pattern in addition to the temperature and longitudinal strain of the fiber. An FBG behaves as Bragg reflector, hence, transmits some wavelengths and reflects others (wavelength's peak of the FBG) depending on its grating period. Since the reflected wavelength changes with temperature and strain variations, it is possible to sense these variations by tracking the FBG's peak (see Figure 1). The following equation represents the mathematical relationship between temperature and strain changes and the shift of an FBG's peak[43]:

$$\frac{\Delta\lambda}{\lambda_0} = (1 - p_{\text{eff}})\Delta\varepsilon + (\alpha + \xi)\Delta T, \tag{1}$$

where $\Delta\lambda$, λ_0, $\Delta\varepsilon$, and ΔT are the wavelength change, the wavelength value and the strain, and temperature variations. The parameters p_{eff}, α, and ξ are the photoelastic coefficient, the thermal expansion coefficient, and the thermal-optic coefficient, respectively.

In view of the foregoing, when optical fiber strain sensors are used for SHM, an efficient transition of the strain between the structure under scrutiny (host structure) and the core of the optical fiber is required. Hence, an adequate bonding, at the material point where the strain is sensed, is of paramount importance to guarantee the accurate evaluation of the state of strain.
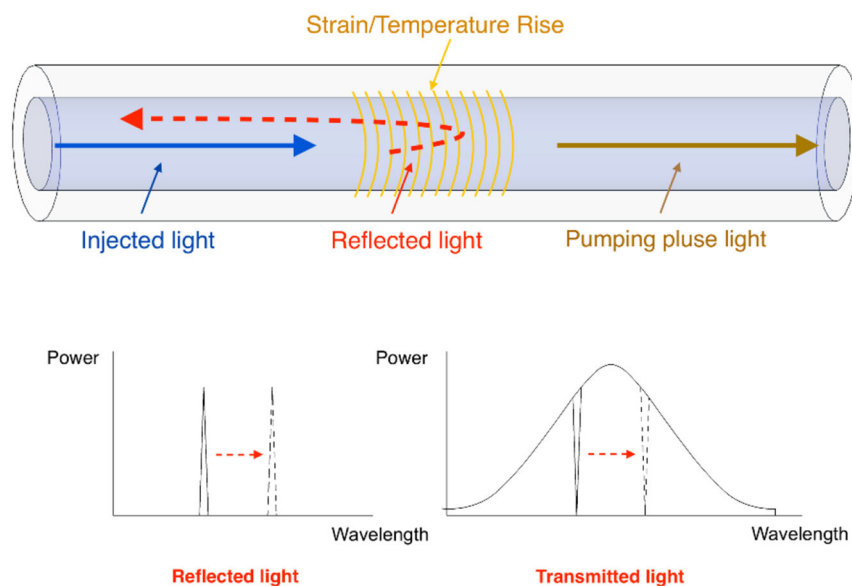

FIGURE 1 Sensing principle of fiber Bragg grating sensor

3 | LIMITATIONS OF THE PREVIOUS ANALYSES ON BONDING STRAIN TRANSFER

In the *strain measurements* techniques, the most common method of sensor application is bonding. This method is simple and cost-effective and allows repairability and easy inspectionability of the sensors. On the other hand, the strain measured by a surface-bonded sensor does not coincide with the effective strain of the host material. Due to the shear deformation absorbed from protective coating and adhesive layers, the optical fiber strain measured is different from that of the host materials. This phenomenon is one of the principal disadvantages of surface strain sensors and, hence, also OFSs. Many factors that influence strain transfer have been identified in the literature. The reliability of an OFS in measuring structural strain particularly depends on its bonding characteristics, which include (i) bonding length, (ii) bonding transversal width, (iii) size of the lower and upper layer of the adhesive with respect to the fiber position, (iv) the glue's mechanical properties, (v) coating's mechanical properties, and (vi) the mechanical properties of the host material. Many researchers have studied strain transmission loss by analytical models, numerical simulations, and experimental tests.

The following subsections describe the main research and findings on the principal parameters that influence strain transfer efficiency in bonded OFSs.

3.1 | Bonding length analysis

Several analytical models have demonstrated that strain transmission varies as a function of the bonding length. Her and Tsai studied bonded fiber optic sensors and developed three research approaches under the hypotheses of linear elasticity and perfect bonding.[44] First, an analytical formula was proposed, and a numerical study was carried out together with experimental tests. These three methods agreed that the greater the bonding length is, the better the strain transmission efficiency is. Based on a similar hypothesis, Wan et al. built an analytical model[41] and validated it by applying the extended Fourier amplitude sensitivity test.[45] Her and Huang also confirmed the influence of bonding length through analytical FEAs,[39,46] while Wan et al. made an in-depth study of the influence of the coating on bonding length.[41]

3.2 | Layers' thickness analyses

The thickness of the adhesive is another influential parameter in strain monitoring analysis. Wan et al. analyzed different upper thickness and proved that the bonding efficiency is insensitive to this parameter.[41] For coated fibers, the strain transfer efficiency gradually declines with increasing upper thickness but so slowly that it does not have a major effect on the strain transfer in practice.[41] On the other hand, Torres et al. developed a 3D finite element (FE) model considering an optical fiber covered with resin packaging and positioned it on a layer of adhesive to investigate the influence of the lower adhesive thickness.[47] This study revealed an inverse mathematical relationship between lower adhesive thickness and the percent of strain transferred. The research of Li et al. later confirmed this assumption.[48] Not only bonding length determines the improvement of strain transfer, but this latter also notably increases as the thickness of the adhesive layer is reduced.[42]

3.3 | Width's analysis

For an exhaustive review of the geometrical parameters of an OFS's attachment, the width of the bonding should be included. Wan et al.[41] analyzed the influence of width and concluded that bonding efficiency is insensitive to width, as it was the case for coated fibers and bare fibers. Li et al.[48] confirmed this conclusion and did not find a strong relationship between strain transfer efficiency and width.

3.4 | Stiffness of materials' analyses

Other parameters that influence FBG bonding's effectiveness are the mechanical characteristics of the adhesive, coating, and host material. One of the first studies that correlated the stiffness of the components and the strain transfer loss was carried out by Torres et al.,[47] who found that sensor efficiency varied with Poisson's ratio.

The influence of the mechanical characteristics of the adhesive was studied from a theoretical point of view by Li et al.,[42] Pak,[49] and Her and Tsai,[44] who also analyzed the effectiveness of fiber optic sensor bonding as a function of adhesive stiffness and defined an analytical formula to predict the phenomenon. These studies showed that strain transfer increases with an increasing adhesive elastic modulus. Li et al. found that the average strain transfer rate (efficiency of the sensor bonding) improves with increasing elasticity's modulus of the adhesive layer.[42] Other authors[48] thus proposed to replace organic with metal adhesives to optimize FBG performance, although this solution involves a series of operational difficulties.

3.5 | Limitations of previous analyses

Several authors have studied various parameters related to strain transfer losses in FBGs and identified the mathematical relations between some of these parameters and the strain transfer efficiency. Various analytical models have also been developed to try to predict the influence of some combinations of these parameters.

However, there is still a need for a simultaneous analysis of all the parameters with a comprehensive 3D FEA. In addition, guidelines and exhaustive best practices for a correct bonding of OFSs would be extremely useful to minimize the problems associated with strain transfer losses in future OFS applications.

The present study aspires to provide the most comprehensive analysis of strain transfer in surface-bonded FBGs, taking into account all the parameters at once. Hence, Table 1 emphasize the completeness of the proposed work in comparison with the previous studies that only investigated single aspects of the phenomenon by means of different approaches.

4 | FINITE ELEMENT ANALYSIS

With the aim of achieving a complete understanding of the parameters that influence surface-bonded OFSs' efficiency in sensing strain, a series of FEAs of bonding was undertaken by using SIMULIA ABAQUS software.[52]

4.1 | FE models geometry

Each model was composed of several parts: (i) the support representing the portion of the structure to which the sensor is bonded; (ii) the glue that bonds sensor and support; (iii) the optical fiber, including core and cladding; and (iv) in some cases the coating, a protective layer surrounding the fiber. The upper surface of the glue is shaped in a truncated elliptical cylinder to mimic the natural shape taken by liquid glue due to surface tension. Taking advantage of the plane of symmetry, the models are cut in the middle longitudinally to reduce computation time and complexity.

Figure 2 illustrates the geometry of the model and defines the geometrical parameters taken into account in the analyses:

- t: upper thickness of adhesive,
- T: lower thickness of adhesive,
- W: width of bonding, and
- L: length of bonding.

The materials considered were assumed to be solid and homogeneous and have perfectly elastic behavior. In each simulation, a displacement along the longitudinal direction was imposed at one end of the support, while the other end was constrained, so that a uniaxial tensile deformation equal to 1% was induced in the structural element. The different parts of the model were held together by tie constraints, whereby the longitudinal tensile deformation propagated from the support to the optical fiber. Finally, the measurable strain was considered as the longitudinal deformation of the fiber, since it behaved as an intrinsic strain sensor.

Before meshing the designed geometry, the edges of the fiber were seeded by prescribing the elements' size in order to guarantee the correct mesh transition, despite the small fiber diameter. The mesh was automatically generated by the ABAQUS mesh algorithm using three-dimensional triangular prism elements. The six-node wedge element, C3D6,

TABLE 1 Parametrical analyses' state of art: relevant research

Parameters and approaches		Current work	Her and Huang[39]	Davidi et al.[50]	Wan[51]	Her and Huang[46]	Li et al.[48]	Her and Tsai[44]	Pak[49]	Li et al.[42]	Wan et al.[41]	Torres et al.[47]
Parameters	Bonding length	x	x		x	x	x	x			x	
	Bonding width	x					x				x	
	Adhesive thickness	x					x		x	x	x	x
	Materials mechanical properties	x	x	x	x	x	x	x	x	x		x
Coating	Coated fiber	x	x	x	x	x		x	x	x	x	
	Bare fiber	x					x		x	x	x	x
Approaches	Analytical	x	x		x	x	x	x	x	x	x	
	FEM	x	x	x				x			x	x
	Experimental	x	x	x	x	x		x				

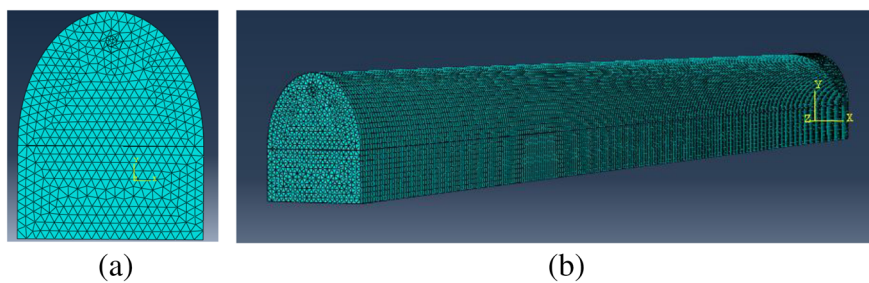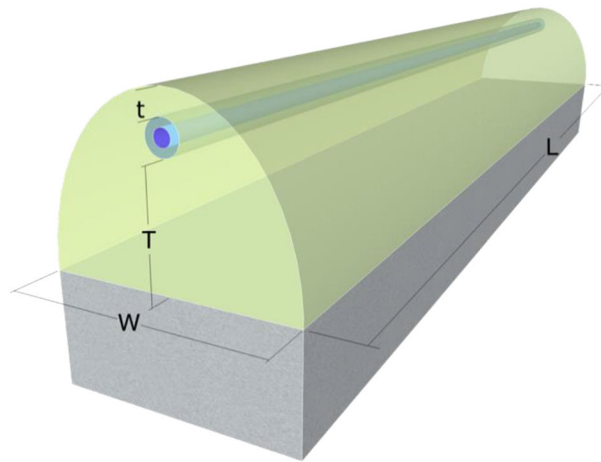**FIGURE 2** Geometrical parameters of the bonding

FIGURE 3 (a) Transversal view of model mesh and (b) overall view of model mesh

was selected as the most suitable to ensure the efficient match of the model with the complex curved geometry of the problem and limit computational complexity. The mesh adopted is shown in Figure 3.

The purpose of the FEAs was to study the efficiency of different bonding configurations calculated as a percentage of the longitudinal strain of the optical fiber compared with the strain imposed on the support, using the following equation:

$$\Delta = \frac{\varepsilon_f(-)}{\varepsilon_s(-)} \cdot 100 \ (\%), \tag{2}$$

where Δ is the *efficiency* and ε_f and ε_s are, respectively, the average values of longitudinal strain of the fiber along the sensing length, considered at the center of the bonding length and equal to 5.0 mm, and the longitudinal strain of the support.

4.2 | FEA inputs

One hundred seventeen FEAs were carried out to identify the parameters that influence *efficiency* and determine their effects on the strain transfer.

4.2.1 | Effects of bonding geometry

As several studies have shown the remarkable influence of the bonding geometry on strain transfer efficiency,[39,41,42,47,48,50,51] an extensive investigation was thus focused on this aspect.

Table 2 illustrates the mechanical characteristics of the material used as FEA inputs. The optical fiber had the standard diameter of 125 μm and was made of silica. The coating outer diameter was 250 μm (the inner diameter was not

defined since equal to fiber diameter). The support was made of steel, one of the most common materials in civil and mechanical engineering applications.

One hundred seventeen different FE models were developed by varying the bonding geometry. Sixty-nine FE models studied the influence of L, T, t, and W on the efficiency of bare fiber bonding, combining the geometrical parameters listed in Table 3. Forty-eight FE models were designed by combining the parameters listed in Table 4 to study bonding efficiency in strain transfer of coated OFSs. In this last case, the width of the bonding was ignored to reduce computation time, since its influence on the phenomenon was proved to be insignificant.

4.2.2 | Effects of materials stiffness

Another interesting aspect that influences strain transfer efficiency between support and optical sensor is the difference between the stiffness of the structural element to which the sensor is bonded and the stiffness of the coating and adhesive, which transmit the strain to the optical fiber. A series of FE models were developed taking into consideration supports with different Young's modulus, as listed in Table 5.

Geometrical and mechanical parameters	Values	Units
Fiber diameter	125	μm
Coating outer diameter	250	μm
Support Young's modulus	210	GPa
Support Poisson's ratio	0.3	/
Adhesive Young's modulus	2.5	GPa
Adhesive Poisson's ratio	0.3	/
Fiber Young's modulus	70.0	GPa
Fiber Poisson's ratio	0.22	/

TABLE 2 Geometrical and mechanical parameters of the FE models

L (mm)	T (μm)	t (μm)	W (mm)
5	100	0	1
10	200	100	2
20	300	150	5
60	400	200	
	500		
	800		
	1000		

TABLE 3 Geometrical parameters selected to evaluate the efficiency of bare optical fiber sensors

L (mm)	T (μm)	t (μm)
5	100	0
10	200	100
20	300	150
60	400	200
	500	
	800	
	1000	

TABLE 4 Geometrical parameters selected to evaluate the efficiency of coated optical fiber sensors

4.3 | Results

This subsection analyzes the results of the FEAs (reported in full in Appendices A–D). In order to make the research outcomes more fruitful and user-friendly and determine the mathematical relationships between the considered variables, a sequence of models was calibrated by fitting the obtained data with three-variable curves using the Curve Fitting MATLAB® Toolbox™.[53] The model equations can be used to predict the achievable performance of different bonding configurations. In the following subsections, the different three-variable curves obtained are presented and discussed.

4.3.1 | Effects of bonding geometry

Figure 4 shows the relationship between *efficiency* and lower adhesive thickness and bonding width when the bonding length is 20 mm and the upper adhesive thickness 150 μm. The lower adhesive thickness has a remarkable inverse effect on bonding efficiency. As the bonding width seems to only slightly influence it, as shown by previous research,[41,48] it was neglected in the following analysis.

Figure 5 illustrates the relationship between *efficiency* and lower and upper adhesive thickness, when the bonding width and length are 2 and 60 mm, respectively. It should be noted that both these parameters linearly and inversely influence the strain transfer. *T* has a considerably greater effect, as can be seen by the slope of the curve. This outcome is in agreement with previous studies in which the lower adhesive thickness was recognized as playing one of the leading roles in the phenomenon.[41,42,47–50]

The comparison of bonding performance, lower adhesive thickness, and bonding length for a bare and coated OFS is shown in Figure 6, in which the upper adhesive thickness is 100 μm and the bonding width 2 mm.

The bonding length and the lower adhesive thickness were found to be the most significant variables, in agreement with previous studies.[41,42,44–48] While the relationship between lower adhesive thickness and bonding efficiency was once again inversely proportional, bonding length directly affected the *efficiency*. The comparison of the results of the analyses with bare fiber and coated fiber shows that the coating has a negative effect on strain transfer efficiency.

TABLE 5   Input parameters for materials stiffness analyses

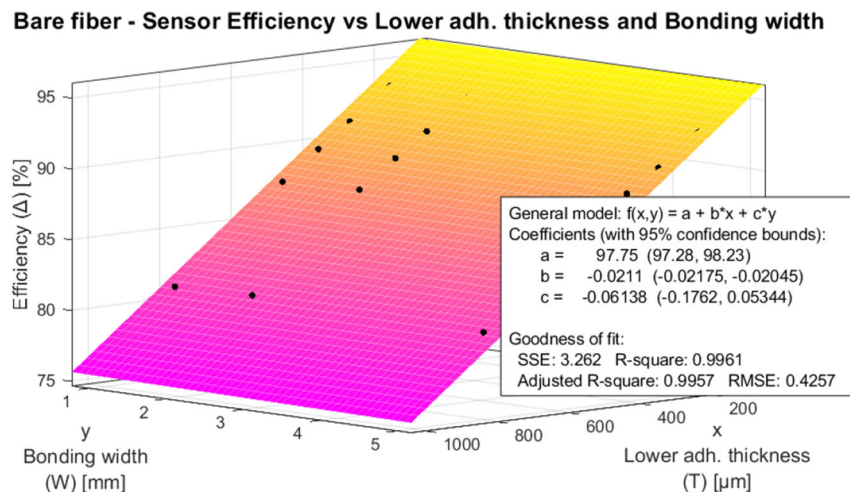| Materials stiffness							
$T = 400$ μm; $t = 150$ μm; $L = 30$ mm							
Coating (GPa)	Adhesive (GPa)	Support (GPa)					
3.0	2.5	16	20	30	45	73	100	210

FIGURE 4   Curve fitting—relationship between strain transfer efficiency and lower adhesive thickness and bonding width
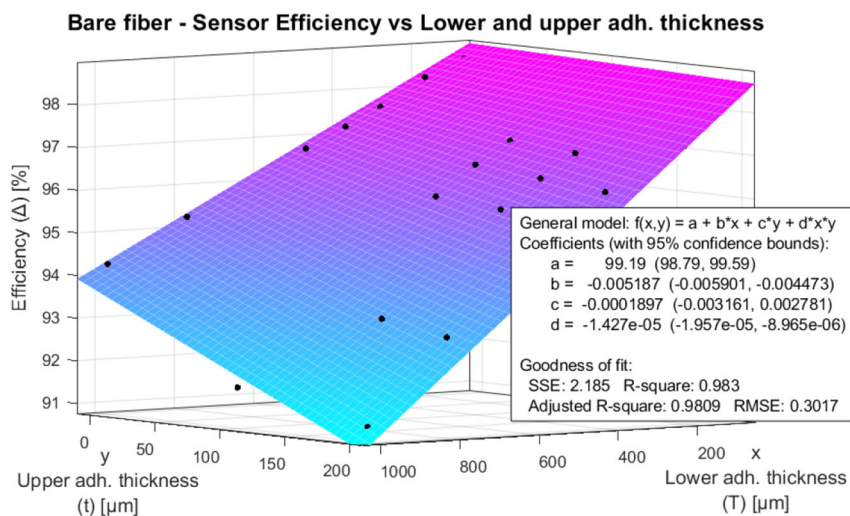
FIGURE 5 Curve fitting—relationship between strain transfer efficiency and lower and upper adhesive thickness

4.3.2 | Effects of materials stiffness

Figure 7 shows the relationship between material stiffness and bonding efficiency when $T = 400$ µm, $t = 150$ µm; $L = 60$ mm and $W = 2$ mm. The performance of the bonding strongly depends on the stiffness of the host material, with a power–function relationship. To better understand the results of the FEAs, the Young's modulus ratio, r, was obtained from the following equation:

$$r = \frac{E_{\text{support}}}{\min\left(E_{\text{adhesive}}; E_{\text{coating}}\right)} \qquad [-], \tag{3}$$

where E_{support}, E_{adhesive}, and E_{coating} are, respectively, the modulus of elasticity of support, adhesive, and coating.

The best performance was obtained when the Young's modulus of the support was about 10 times higher than the minimum between the ones of coating and adhesive, while the strain transfer efficiency rapidly decreases and becomes unsatisfactory when r is below 2. These aspects become critical when OFSs are bonded to soft materials, such as plastic.

4.4 | Guidelines for choosing optimal bonding

This section summarizes the results of the FEAs and provides practical guidelines for the manufacture of efficient optical fiber bonding. Figure 7 shows the values considered in this research work for the geometrical and mechanical parameters of the bonding and the corresponding performance expressed according to a qualitative scale: good (green), satisfactory (yellow), and poor (red) performance. Sometimes, it may be difficult to manually produce bonding with some of the values of the geometric parameters considered here. To stress this potential drawback, the geometric parameters with possible operational difficulties are highlighted in gray in the guidelines (Figure 8). To provide an example, even if bonding length positively affects strain transfer performance, the bonding heterogeneity can increase with length. A similar drawback and operational difficulty can occur for very thin layer of adhesive. It is worth mentioning that a gradient of strain in the area where the FBG is located can produce a peak splitting in the FBG reflection spectrum, significantly reducing the accuracy in strain sensing. Therefore, when the state of strain the host structure is not uniform, it is opportune to increase the bonding length in order to reduce the gradient of strain along the FBG length.

(a)

(b)
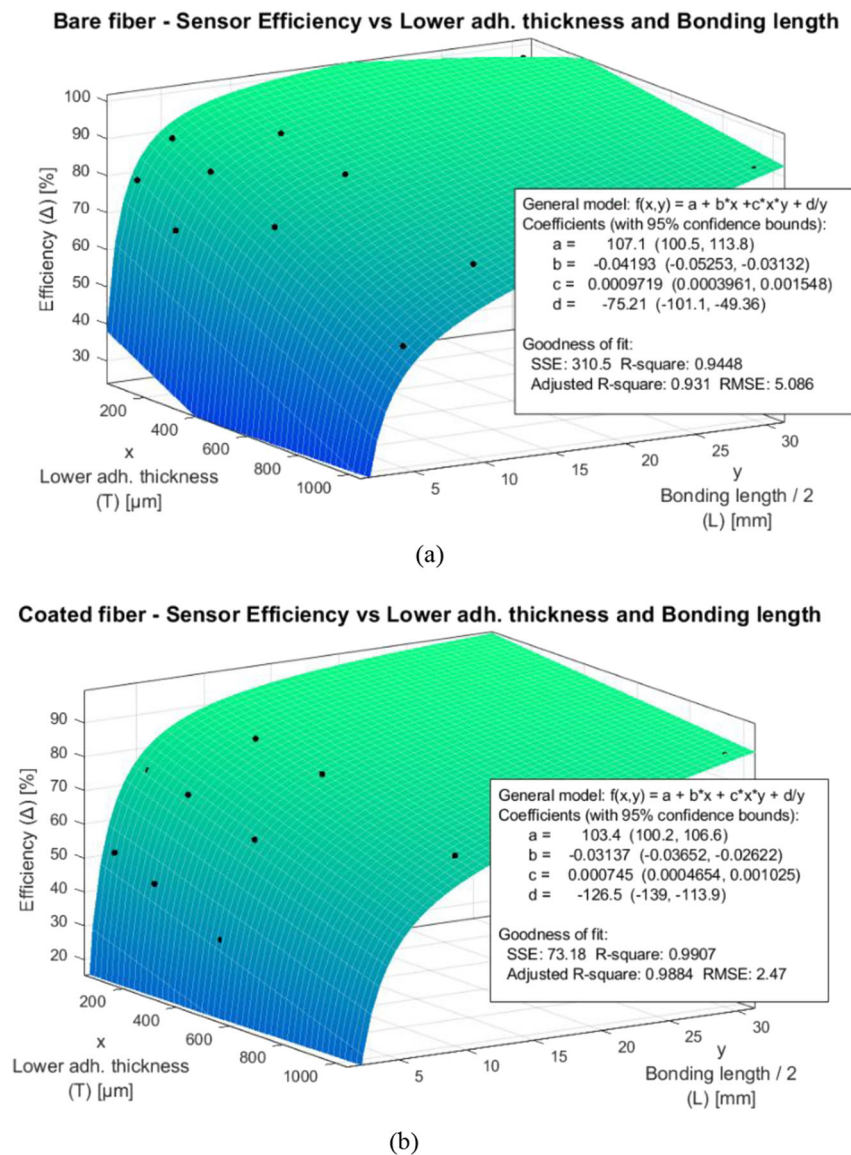
FIGURE 6 Curve fitting—relationship between strain transfer performance and lower adhesive thickness and the bonding length for (a) bare optical fiber sensors and (b) coated optical fiber sensor

5 | VALIDATION TEST

The experimental phase consisted of the pure tension test of a specimen plate made of steel (host material) on which three FBGs were bonded with a bicomponent epoxy adhesive. This was designed to verify that the 3D FEAs effectively simulate actual sensor behavior and strain transmission mechanism and to confirm the importance of the main parameters identified (bonding length and bonding lower thickness). For this purpose, three different bondings, with different geometric features, were produced and tested in the ICITECH laboratory of the *Universitat Politècnica de València* (UPV). The optical sensor production, the experimental setup, and the results are reported below.

5.1 | Experiment setup

The validation test was carried out at the UPV's ICITECH. The experimental setup consisted of (i) the specimen, (ii) the tensile test apparatus, (iii) three FBGs, and (iv) the fiber optic interrogator.
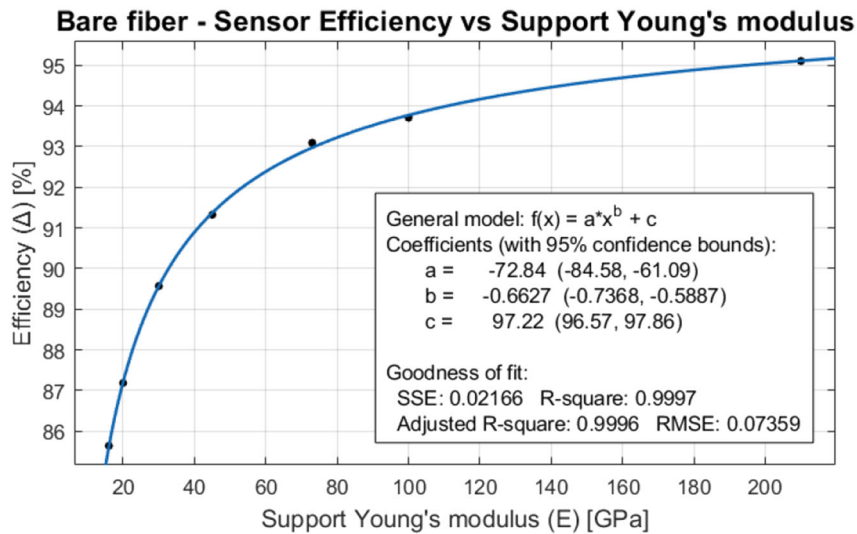
FIGURE 7   Bonding efficiency related to support stiffness

Bare fiber	Lower adhesive thickness [μm]	> 500	300-500	100-300	<100
	Bonding length [mm]	< 10	10-20	20-50	>50
Coated Fiber	Lower adhesive thickness [μm]	> 400	200-400	100-400	<100
	Bonding length [mm]	< 14	14-24	24-50	>50
Young's Modulus ratio [-]		< 2	2-3	> 3	
Upper adhesive thickness [μm]		little improvements at decreasing upper adhesive thickness			
Bonding width [mm]		irrelevant			

FIGURE 8   Guidelines for the correct bonding manufacturing

5.1.1 | Specimen

The specimen was a 360 mm × 40 mm × 10 mm plate. The material was steel 235 (yield strength 0.235 GPa and Young's modulus 210 GPa).

  The adhesive was bicomponent epoxy "Araldite," a cold reaction thermosetting polymer. The two components were a base resin (component A) and a hardener (component B), which give rise to a glossy vitrified layer when mixed. Curing time was about 24 h, Young's modulus 3.1 GPa, and the Poisson's ratio 0.3. Such adhesive was selected because its Young's modulus was on the center of the range of values reported in the previous studies.[39,41,44,46,48]

  Three different bonding configurations were made to verify the effectiveness of the ABAQUS 3D FEAs, obtained by varying bonding length (L) and bonding lower thickness (T). The sensors were glued as close as possible in order to be subjected to a uniform deformation. As the L and T parameters had the greatest effect on bonding effectiveness in the FEM, these parameters were chosen to vary the bonding characteristics in the experimental phase. Table 6 and Figure 9 show the specimen's geometrical and mechanical parameters.

5.1.2 | Tensile test apparatus

A hydraulic tensile test apparatus was used to produce a state of tensile strain (Figure 10). The machine stretched the specimen in a controlled uniaxial tension strain by means of pistons and grips, while the applied load was obtained by the internal oil pressure. The applied deformation ranged between the deformation corresponding to 10% and 70% of the specimen's yield strength. This was chosen to guarantee the element's mechanical elastic behavior.

TABLE 6 Geometrical and mechanical parameters of the specimen

| Sensor FBG1		Sensor FBG2		Sensor FBG3	
Length (L) (mm)	Lower thickness (T) (μm)	Length (L) (mm)	Lower thickness (T) (μm)	Length (L) (mm)	Lower thickness (T) (μm)
20	500	20	1000	5	500
Mechanical parameters			**Values**		**Units**
Host material—Young's modulus			210		GPa
Host material—Poisson's ratio			0.30		/
Adhesive—Young's modulus			3.1		GPa
Adhesive—Poisson's ratio			0.30		/
Fiber—Young's modulus			70		GPa
Fiber—Poisson's ratio			0.22		/
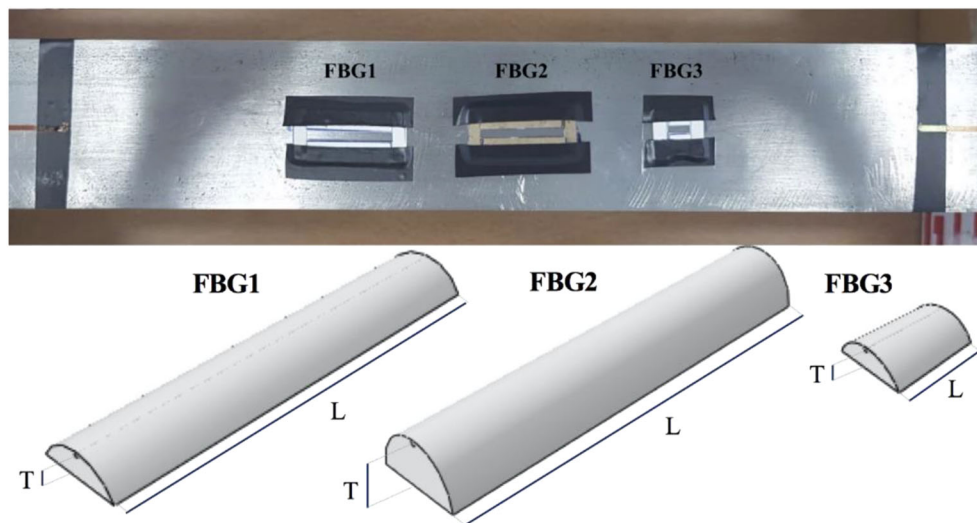
FIGURE 9 Specimen preparation and three bonding configurations of the FBG sensors
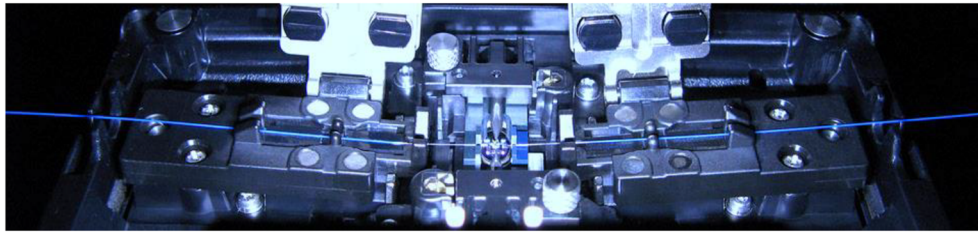
FIGURE 10 Experimental setup
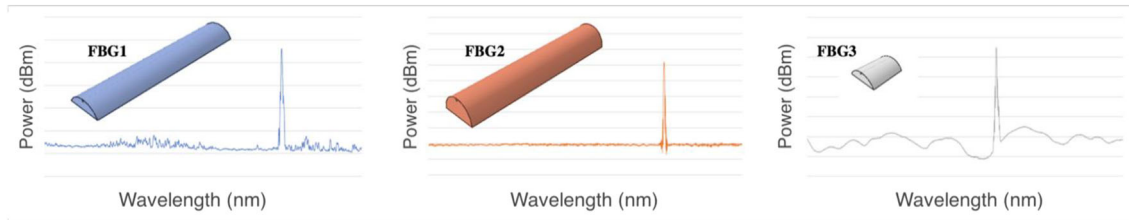
FIGURE 11 Fiber fusion splicer

FIGURE 12 Spectra of reflective wavelength the three FBGs at the instant 0 of experiment

5.1.3 | Fiber optic sensors

The fiber optic sensors were fabricated in the Institute of Telecommunications and Multimedia Applications (iTEAM) of the UPV by inscribing three FBGs in a commercial single-mode optical fiber (mode field diameter of 6.4 μm and a numerical aperture of 0.2). The optical fiber was first hydrogen loaded for 2 weeks at ambient temperature and at 20 bars pressure to enhance its photosensitivity. Then, the phase-mask method was employed to write three 5.0-mm-long gratings by using a 244-nm CW frequency-doubled argon-ion laser with 60-mW output power.

The interrogator used to read the FBGs was a Static Optical Sensing Interrogator—Model sm125 (Micron Optics). Data were read and stored by a portable control unit with Micron Optics ENLIGHT Software. A fusion splicer was used to splice the sensors to optical fiber connectors in order to interrogate them (Figure 11). This device first aligns the two fiber segments and welds the ends by means of an electric arc while automatically controlling the junction efficiency. The goal was to join both parts so that the light passed through them without dispersion or reflection. The transmission light loss through this procedure was approximately 0.1 dB for all three FBG.

5.2 | Experiment setup

The tensile test was carried out by applying a loading–unloading cycle. The maximum load was calculated to keep the host material in the elastic field (60 kN). Starting from zero, a load cycle of 12 load increments (5 kN each) was imposed at intervals of approximately 60 s (total test time was 1434 s).

The wavelength FBG peak shifts, which varied in proportion to fiber stretching, were continuously detected with a frequency data acquisition of 1 Hz on the ENLIGHT software. It was therefore possible to calculate the strain value by determining the relation between wavelength shift and strain, known as the *gage factor*. Figure 12 shows the spectra of the reflective wavelength of the three FBGs at the start of the experiment. It is worth noting that the spectrum of FBG3 (third case in Figure 12) is distorted due to a loose or dirty connector or due to the reflection generated at fiber end. However, this phenomenon has been neglected, since it does not affect the peak tracking.

The strain values of the host material were analytically deduced from the load applied and its mechanical and geometrical characteristics. Figure 13 shows the strain measurement variation over time.

As the FEAs, the validation test provided useful information on the experimental efficiency of the FBG sensors (Δ). This can be evaluated as a percentage of the longitudinal strain of optical fiber along the sensing length (5.0 mm) compared with the strain induced in the support using 2 to immediately extract qualitative considerations. The FBG1 had the greatest efficiency with respect to strain transfer losses (FBG2 and FBG3 were second and third). The *FBG1 strain*

FIGURE 13 Chart of strain measurements (host material and FBG sensors)
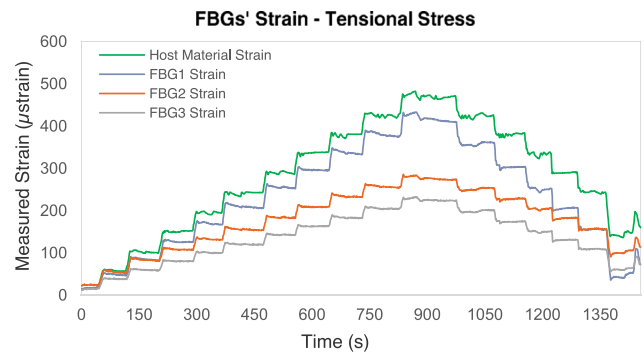
TABLE 7 Comparison of experimental *efficiency* obtained in the validation test and the ones resulting from the ABAQUS 3D FEAs

Configurations	Δ_{FBG1}	Δ_{FBG2}	Δ_{FBG3}
Validation test	81.281	68.496	50.545
FEM 3D ABAQUS	85.875	79.141	52.887

curve in Figure 12 is the most similar to that of the host material. The experiment confirmed (in agreement with the literature[41] and as shown by the 3D FEAs) that bonding efficiency decreases as lower adhesive thickness increases. Bonding length was also confirmed to be a fundamental parameter in reducing efficiency.

Second, the obtained efficiency values can be compared with the efficiency determined by the 3D FEM. In particular, the behavior of FBG1, FBG2, and FBG3 can be compared with that of the FE models by considering the same geometrical configuration and mechanical properties of bonding, fiber, and host material simulated on ABAQUS.

Table 7 shows the values of *efficiency* Δ_{FBG1}, Δ_{FBG2}, and Δ_{FBG1} obtained in the validation test and in the ABAQUS 3D FEAs.

The comparison shows that the experimental test perfectly reflected the ranking and trend of the FEAs outcomes. In fact, as illustrated in Table 7, the outcomes of the numerical models are very similar to those obtained in the experimental test, with an average error of 7%. This demonstrates that, for the three FBG configurations, the ABAQUS model reproduces the phenomenon with good approximation. The authors suppose that the inevitable fiber curving and imperfect adhesive geometry (related to manual glue application) may be the cause of the lower experimental efficiency in comparison with that evaluated on ABAQUS.

6 | CONCLUSIONS

This paper described a numerical and experimental study carried out to investigate the performance of surface bonding of OFSs considering for the first time all the parameters influencing the phenomenon. Recent research on optical fiber bonding was first reviewed, and the significant parameters were identified. An extensive number of FEAs were then performed, considering 117 different FE models, to identify the role in the strain transfer mechanism of the geometrical characteristic of the bonding: bonding length, bonding width, lower thickness adhesive and upper adhesive thickness, and the mechanical properties of the host materials. An experimental study was designed to corroborate the outcomes of the analyses, and the performance of different bonding configurations was assessed by means of quasi-static tensile tests. The research involved a combination of synergistically related techniques and interdisciplinary skills, bonding computational simulation, experimental tests, sensor manufacturing, and data analysis.

It was found that lower adhesive thickness and bonding length are the parameters that most influence bonding performance. The first one influences the bonding performance according to an inversely proportional relationship, whereas the second one with nonlinear proportional relationship. The third parameter that plays an important role in the phenomenon is the ratio between the Young's modulus of the support and those of the coating and the adhesive. The difference between the stiffness of support and that of the other components affects the strain transfer performance with power law, while the contribution of bonding width and upper adhesive thickness were shown to be, respectively, irrelevant and almost negligible. It is worth mentioning that the coating proved to have a negative effect on strain

transfer efficiency. The mathematical relationships between the considered parameters and the strain transfer performance were determined by three-variable functions, fitting the FEA outcomes. The equations of these curves can be used as predictive models to determine the achievable performance of different bonding configurations.

To conclude, some practical guidelines for the correct manufacturing of surface bonding of OFSs were given based on the results of the study. These powerful instruments can help both the research community and industry to improve the performance of surface-bonded optical fiber strain sensors and, hence, enhance the performance of SHM systems.

Thanks to the extensive FEAs, which allowed a comprehensive investigation of the role played by all the significant parameters, this research overcomes the limits of previous analyses and, synthesizing the outcomes, provides a practical guide for efficient use of surface-bonded optical fiber strain sensors. It also highlights several issues resulting from the manual production of surface bonding.

Future research will focus on a deep investigation on the influence of the adhesive on the performance of optical fiber strain sensors, considering different typologies, such as monocomponent and bicomponent with diverse curing times and mechanical characteristics, and taking into account both the efficiency and the simplicity of application. Moreover, the most suitable type of adhesive and an automated production of OFS bonding with high-precision numerically controlled devices will be used to improve the sensors' performances.

AUTHOR CONTRIBUTIONS

Ignazio Floris conducted the investigation and prepared the original draft of the manuscript. Valentino Sangiorgio conducted the investigation and prepared the original draft of the manuscript. José M. Adam supervised the study and reviewed and edited the manuscript. Giuseppina Uva conducted the investigation and conceptualized the study. Monica Rapido conducted the investigation and prepared the software. Pedro A. Calderón provided the resources and supervised the study. Javier Madrigal conducted the investigation and the formal analysis.

ORCID

José M. Adam   https://orcid.org/0000-0002-9205-8458

REFERENCES

1. Mattei NJ. Infrastracture Report Card 2017: a comprehensive assesment of Americas's infrastructure. *ASCE*. 2017;1-112.
2. López-Higuera JM, Cobo LR, Incera AQ, Cobo A. Fiber optic sensors in structural health monitoring. *J Lightwave Technol*. 2011;29(4): 587-608. https://doi.org/10.1109/JLT.2011.2106479
3. Krajewski JE. Bridge inspection and monitoring 2006: 455–456. https://doi.org/10.1201/b18175-184
4. Feng D, Feng MQ. Computer vision for SHM of civil infrastructure: from dynamic response measurement to damage detection—a review. *Eng Struct*. 2018;156:105-117. https://doi.org/10.1016/j.engstruct.2017.11.018
5. Sangiorgio V, Uva G, Fatiguso F. User reporting–based semeiotic assessment of existing building stock at the regional scale. *J Perform Constr Facil*. 2018;32(6):1-14. https://doi.org/10.1061/(ASCE)CF.1943-5509.0001227
6. Sangiorgio V, Uva G, Adam JM, Scarcelli L. Failure analysis of reinforced concrete elevated storage tanks. *Eng Fail Anal*. 2020; 115(May):104637. https://doi.org/10.1016/j.engfailanal.2020.104637
7. Sangiorgio V, Uva G, Adam JM. Integrated seismic vulnerability assessment of historical masonry churches including architectural and artistic assets based on macro-element approach. *Int J Architect Herit*. 2020;3058:1-14. https://doi.org/10.1080/15583058.2019.1709916
8. Sangiorgio V, Uva G, Aiello MA. A multi-criteria-based procedure for the robust definition of algorithms aimed at fast seismic risk assessment of existing RC buildings. *Structure*. 2020;24:766-782. https://doi.org/10.1016/j.istruc.2020.01.048
9. Hiasa S. Investigation of infrared thermography for subsurface damage detection of concrete structures 2016.
10. Sabato A, Niezrecki C, Fortino G. Wireless MEMS-based accelerometer sensor boards for structural vibration monitoring: a review. *IEEE Sens J*. 2017;17(2):226-235. https://doi.org/10.1109/JSEN.2016.2630008
11. Matveenko VP, Shardakov IN, Voronkov AA, et al. Measurement of strains by optical fiber Bragg grating sensors embedded into polymer composite material. *Struct Control Health Monit*. 2018;25(3):e2118. https://doi.org/10.1002/stc.2118
12. Liu W, Wang H, Zhou Z, Xing X, Cao D, Jiang Z. Optical fiber-based sensors with flexible encapsulation for pavement behavior monitoring. *Struct Control Health Monit*. 2015;22(2):301-313. https://doi.org/10.1002/stc.1674

13. Chang FK. Ultra reliable and super safe structures for the new century. In Proceedings of the First European Workshop of Structural Healt Monitoring, 2002.

14. Porcu MC, Pieczonka L, Frau A, Staszewski WJ, Aymerich F. Assessing the scaling subtraction method for impact damage detection in composite plates. *J Nondestr Eval.* 2017;36(2):33. https://doi.org/10.1007/s10921-017-0413-9

15. Porcu MC, Patteri DM, Melis S, Aymerich F. Effectiveness of the FRF curvature technique for structural health monitoring. *Construct Build Mater.* 2019;226:173-187. https://doi.org/10.1016/j.conbuildmat.2019.07.123

16. Frau A, Pieczonka L, Porcu MC, Staszewski WJ, Aymerich F. Analysis of elastic nonlinearity for impact damage detection in composite laminates. *J Phys Conf Ser.* 2015;628(1):012103. https://doi.org/10.1088/1742-6596/628/1/012103

17. Lee B. Review of the present status of optical fiber sensors. *Opt Fiber Technol.* 2003;9(2):57-79. https://doi.org/10.1016/S1068-5200(02)00527-8

18. Annamdas KKK, Annamdas VGM. Review on developments in fiber optical sensors and applications. In: Mendez A, Du HH, Wang A, Udd E, Mihailov SJ, eds. *Fiber Optic Sensors and Applications VII*, vol. 7677, 2010. https://doi.org/10.1117/12.849799

19. Barrera D, Madrigal J, Delepine-Lesoille S, Sales S. Multicore optical fiber shape sensors suitable for use under gamma radiation. *Opt Express.* 2019;27(20):29026-29033. https://doi.org/10.1364/OE.27.029026

20. Hongo A, Kojima S, Komatsuzaki S. Applications of fiber Bragg grating sensors and high-speed interrogation techniques. *Struct Control Health Monit.* 2005;12(3–4):269-282. https://doi.org/10.1002/stc.70

21. Beisenova A, Issatayeva A, Tosi D, Molardi C. Fiber-optic distributed strain sensing needle for real-time guidance in epidural anesthesia. *IEEE Sens J.* 2018;18(19):8034-8044. https://doi.org/10.1109/JSEN.2018.2865220

22. Lombillo I, Blanco H, Villegas L, Boffill Y. Laboratory validation of the hole-drilling technique on the most common load-bearing walls used in heritage constructions. *Construct Build Mater.* 2018;168:280-294. https://doi.org/10.1016/j.conbuildmat.2018.02.069

23. Madrigal J, Barrera D, Sales S. Refractive index and temperature sensing using inter-core crosstalk in multicore fibers. *J Lightwave Technol.* 2019;37(18):4703-4709. https://doi.org/10.1109/JLT.2019.2917629

24. Salazar-Serrano LJ, Barrera D, Amaya W, et al. Enhancement of the sensitivity of a temperature sensor based on fiber Bragg gratings via weak value amplification. *Opt Lett.* 2015;40(17):3962-3965. https://doi.org/10.1364/OL.40.003962

25. Zheng D, Cai Z, Floris I, et al. Temperature-insensitive optical tilt sensor based on a single eccentric-core fiber Bragg grating. *Opt Lett.* 2019;44(22):5570-5573. https://doi.org/10.1364/OL.44.005570

26. Sultangazin A, Kusmangaliyev J, Aitkulov A, Akilbekova D, Olivero M, Tosi D. Design of a smartphone plastic optical fiber chemical sensor for hydrogen sulfide detection. *IEEE Sens J.* 2017;17(21):6935-6940. https://doi.org/10.1109/JSEN.2017.2752717

27. Floris I, Sales S, Calderón PAPA, Adam JMJM. Measurement uncertainty of multicore optical fiber sensors used to sense curvature and bending direction. *Measurement.* 2019;132:35-46. https://doi.org/10.1016/j.measurement.2018.09.033

28. Madrigal J, Barrera D, Hervás J, Chen H, Sales S. Directional curvature sensor based on long period gratings in multicore optical fiber. Proc. SPIE 10323, 25th International Conference on Optical Fiber Sensors 2017:103233A. https://doi.org/10.1117/12.2264920

29. Barrera D, Madrigal J, Sales S. Long period gratings in multicore optical fibers for directional curvature sensor implementation. *J Lightwave Technol.* 2018;36(4):1063-1068. https://doi.org/10.1109/JLT.2017.2764951

30. Zheng D, Madrigal J, Chen H, Barrera D, Sales S. Multicore fiber-Bragg-grating-based directional curvature sensor interrogated by a broadband source with a sinusoidal spectrum. *Opt Lett.* 2017;42(18):3710-3713. https://doi.org/10.1364/OL.42.003710

31. Floris I, Calderón PA, Sales S, Adam JM. Effects of core position uncertainty on optical shape sensor accuracy. *Measurement.* 2019;139:21-33. https://doi.org/10.1016/j.measurement.2019.03.031

32. Floris I, Madrigal J, Sales S, Adam JM, Calderón PA. Experimental study of the influence of FBG length on optical shape sensor performance. *Opt Lasers Eng.* 2020;126:105878. https://doi.org/10.1016/j.optlaseng.2019.105878

33. Khan F, Denasi A, Barrera D, Madrigal J, Sales S, Misra S. Multi-core optical fibers with Bragg gratings as shape sensor for flexible medical instruments. *IEEE Sens J.* 2019;19(14):5878-5884. https://doi.org/10.1109/JSEN.2019.2905010

34. Floris I, Adam JM, Calderòn PA, Sales S. Measurement uncertainty of 7-core multicore fiber shape sensors. In: Kalli K, Brambilla G, O'Keeffe SO, eds. *Seventh European Workshop on Optical Fibre Sensors*, SPIE; 2019. https://doi.org/10.1117/12.2539421

35. Floris I, Adam JM, Calderón PA, Sales S. Fiber optic shape sensors: a comprehensive review. *Opt Lasers Eng.* 2021;139:106508. https://doi.org/10.1016/j.optlaseng.2020.106508

36. Majumder M, Gangopadhyay TK, Chakraborty AK, Dasgupta K, Bhattacharya DK. Fibre Bragg gratings in structural health monitoring—present status and applications. *Sens Actuator A Phys.* 2008;147(1):150-164. https://doi.org/10.1016/j.sna.2008.04.008

37. Pei HF, Teng J, Yin JH, Chen R. A review of previous studies on the applications of optical fiber sensors in geotechnical health monitoring. *Measurement.* 2014;58:207-214. https://doi.org/10.1016/j.measurement.2014.08.013

38. Huang Y, Bao Y, Chen G, Zhou Z. A constrained cylinder model of strain transfer for packaged fiber Bragg grating sensors embedded in inelastic medium. *Struct Control Health Monit.* 2019;26(5):e2335. https://doi.org/10.1002/stc.2335

39. Her SC, Huang CY. Effect of coating on the strain transfer of optical fiber sensors. *Sensors.* 2011;11(7):6926-6941. https://doi.org/10.3390/s110706926

40. Barrias A, Casas JR, Villalba S. Distributed optical fibre sensors in concrete structures: performance of bonding adhesives and influence of spatial resolution. *Struct Control Health Monit.* 2019;26(3):e2310. https://doi.org/10.1002/stc.2310

41. Wan KT, Leung CKY, Olson NG. Investigation of the strain transfer for surface-attached optical fiber strain sensors. *Smart Mater Struct.* 2008;17(3). https://doi.org/10.1088/0964-1726/17/3/035037

42. Li J, Zhou Z, Ou J. Interface strain transfer mechanism and error modification for adhered FBG strain sensor. In: Kulchin YN, Vitrik OB, Stroganov VI, eds. *Fundamental Problems of Optoelectronics and Microelectronics II*, vol. 5851, 2005. https://doi.org/10.1117/12.634066

43. Hong C, Yuan Y, Yang Y, Zhang Y, Abro ZA. A simple FBG pressure sensor fabricated using fused deposition modelling process. *Sens Actuator A Phys*. 2019;285:269-274. https://doi.org/10.1016/j.sna.2018.11.024

44. Her SC, Tsai CY. Strain measurement of fiber optic sensor surface bonding on host material. *Trans Nonferrous Met Soc Chin*. 2009;19 (SUPPL. 1):s143-s149. https://doi.org/10.1016/S1003-6326(10)60262-2

45. McRae GJ, Tilden JW, Seinfeld JH. Global sensitivity analysis—a computational implementation of the Fourier amplitude sensitivity test (FAST) 1980.

46. Her SC, Huang CY. The effects of adhesive and bonding length on the strain transfer of optical fiber sensors. *Appl Sci*. 2016;6(1):13. https://doi.org/10.3390/app6010013

47. Torres B, Payá-Zaforteza I, Calderón PA, Adam JM. Analysis of the strain transfer in a new FBG sensor for Structural Health Monitoring. *Eng Struct*. 2011;33(2):539-548. https://doi.org/10.1016/j.engstruct.2010.11.012

48. Li H, Zhu L, Dong M, Lou X, Guo Y. Analysis on strain transfer of surface-bonding FBG on Al 7075-T6 alloy host. *Optik*. 2016;127(3): 1233-1236. https://doi.org/10.1016/j.ijleo.2015.10.227

49. Pak YE. Longitudinal shear transfer in fiber optic sensors. *Smart Mater Struct*. 1992;1(1):57-62. https://doi.org/10.1088/0964-1726/1/1/008

50. Davidi R, Ben-Simon U, Shoham S, Kressel I, Gorbatov N, Tur M. The importance of fiber coating and bonding process in accurate high spatial resolution strain measurements. 26th International Conference on Optical Fiber Sensors, Optical Society of America; 2018. https://doi.org/10.1364/OFS.2018.ThB4

51. Wan KT. Quantitative sensitivity analysis of surface attached optical fiber strain sensor. *IEEE Sens J*. 2014;14(6):1805-1812. https://doi.org/10.1109/JSEN.2014.2303145

52. Abaqus Unified FEA—SIMULIA™ by Dassault Systèmes®.

53. MATLAB R2015a, The MathWorks, Inc., Natick, Massachusetts, United States.

APPENDIX A: RESULTS OF THE FEAs—EFFECTS OF LOWER ADHESIVE THICKNESS AND BONDING WIDTH ON THE STRAIN TRANSFER EFFICIENCY OF A BARE OPTICAL FIBER SENSOR

Sensor efficiency—effects of bonding width and lower adhesive thickness			
$E_{support} = 210$ GPa; $E_{adhesive} = 2.5$ GPa; $t = 150$ μm; $L = 20$ mm			
Analysis No. (–)	T (μm)	W (mm)	Δ (%)
1	100.00	1.00	95.11
2	200.00	1.00	93.30
3	300.00	1.00	91.14
4	400.00	1.00	89.48
5	500.00	1.00	87.50
6	800.00	1.00	81.06
7	1000.00	1.00	75.92
8	100.00	2.00	95.02
9	200.00	2.00	93.19
10	300.00	2.00	91.21
11	400.00	2.00	89.60
12	500.00	2.00	87.69
13	800.00	2.00	81.20
14	1000.00	2.00	76.18
15	100.00	5.00	94.94
16	200.00	5.00	93.05
17	300.00	5.00	90.89
18	400.00	5.00	89.34
19	500.00	5.00	87.39
20	800.00	5.00	80.84
21	1000.00	5.00	75.63

APPENDIX B: RESULTS OF THE FEAs—EFFECTS OF THE ADHESIVE THICKNESS AND BONDING LENGTH ON THE STRAIN TRANSFER EFFICIENCY OF A BARE OPTICAL FIBER SENSOR

Sensor efficiency—bare optical fiber sensor				
$E_{support} = 210$ GPa; $E_{adhesive} = 2.5$ GPa; $W = 2$ mm				
Analysis No. (–)	L (mm)	T (μm)	t (μm)	Δ (%)
1	5	100.00	0.00	81.42
2	5	100.00	100.00	79.19
3	5	100.00	200.00	77.56
4	5	250.00	0.00	71.80
5	5	250.00	100.00	69.49
6	5	250.00	200.00	67.40
7	5	500.00	0.00	57.36
8	5	500.00	100.00	54.44
9	5	500.00	200.00	52.13
10	5	1000.00	0.00	29.02
11	5	1000.00	100.00	27.34
12	5	1000.00	200.00	25.84
13	10	100.00	0.00	90.13
14	10	100.00	100.00	89.24
15	10	100.00	200.00	88.35
16	10	250.00	0.00	85.40
17	10	250.00	100.00	84.11
18	10	250.00	200.00	82.85
19	10	500.00	0.00	77.51
20	10	500.00	100.00	75.62
21	10	500.00	200.00	74.04
22	10	1000.00	0.00	58.43
23	10	1000.00	100.00	56.58
24	10	1000.00	200.00	54.65
25	20	100.00	0.00	94.98
26	20	100.00	100.00	94.52
27	20	100.00	200.00	94.06
28	20	250.00	0.00	92.56
29	20	250.00	100.00	91.88
30	20	250.00	200.00	91.24
31	20	500.00	0.00	88.43
32	20	500.00	100.00	87.37
33	20	500.00	200.00	86.41
34	20	1000.00	0.00	77.45
35	20	1000.00	100.00	76.17
36	20	1000.00	200.00	74.76
37	60	100.00	0.00	98.28

Sensor efficiency—bare optical fiber sensor				
$E_{support}$ = 210 GPa; $E_{adhesive}$ = 2.5 GPa; W = 2 mm				
Analysis No. (–)	L (mm)	T (μm)	t (μm)	Δ (%)
38	60	100.00	100.00	98.15
39	60	100.00	200.00	97.99
40	60	250.00	0.00	97.49
41	60	250.00	100.00	97.25
42	60	250.00	200.00	97.03
43	60	500.00	0.00	95.99
44	60	500.00	100.00	95.69
45	60	500.00	200.00	95.36
46	60	1000.00	0.00	92.04
47	60	1000.00	100.00	91.52
48	60	1000.00	200.00	90.92

APPENDIX C: RESULTS OF THE FEAs—EFFECTS OF THE ADHESIVE THICKNESS AND BONDING LENGTH ON THE STRAIN TRANSFER EFFICIENCY OF A COATED OPTICAL FIBER SENSOR

Sensor efficiency—coated optical fiber sensor				
$E_{support}$ = 210 GPa; $E_{coating}$ = 3.0 GPa; $E_{adhesive}$ = 2.5 GPa; W = 2 mm				
Analysis No. (–)	L (mm)	T (μm)	t (μm)	Δ (%)
1	5	100.00	0.00	53.75
2	5	100.00	100.00	52.02
3	5	100.00	200.00	51.28
4	5	250.00	0.00	49.20
5	5	250.00	100.00	46.93
6	5	250.00	200.00	45.23
7	5	500.00	0.00	39.80
8	5	500.00	100.00	37.33
9	5	500.00	200.00	35.49
10	5	1000.00	0.00	19.97
11	5	1000.00	100.00	19.13
12	5	1000.00	200.00	17.62
13	10	100.00	0.00	75.87
14	10	100.00	100.00	74.84
15	10	100.00	200.00	73.96
16	10	250.00	0.00	73.24
17	10	250.00	100.00	71.78
18	10	250.00	200.00	70.61

(Continues)

Sensor efficiency—coated optical fiber sensor				
$E_{support} = 210$ GPa; $E_{coating} = 3.0$ GPa; $E_{adhesive} = 2.5$ GPa; $W = 2$ mm				
Analysis No. (–)	L (mm)	T (μm)	t (μm)	Δ (%)
19	10	500.00	0.00	67.30
20	10	500.00	100.00	65.39
21	10	500.00	200.00	63.82
22	10	1000.00	0.00	50.92
23	10	1000.00	100.00	49.15
24	10	1000.00	200.00	47.30
25	20	100.00	0.00	87.71
26	20	100.00	100.00	87.15
27	20	100.00	200.00	86.66
28	20	250.00	0.00	86.31
29	20	250.00	100.00	85.50
30	20	250.00	200.00	84.83
31	20	500.00	0.00	83.03
32	20	500.00	100.00	81.89
33	20	500.00	200.00	80.91
34	20	1000.00	0.00	72.85
35	20	1000.00	100.00	71.51
36	20	1000.00	200.00	70.03
37	60	100.00	0.00	95.85
38	60	100.00	100.00	95.65
39	60	100.00	200.00	95.48
40	60	250.00	0.00	95.37
41	60	250.00	100.00	95.07
42	60	250.00	200.00	94.83
43	60	500.00	0.00	94.20
44	60	500.00	100.00	93.77
45	60	500.00	200.00	93.40
46	60	1000.00	0.00	90.28
47	60	1000.00	100.00	89.70
48	60	1000.00	200.00	89.04

APPENDIX D: RESULTS OF THE FEAs—INFLUENCE OF THE MATERIALS STIFFNESS ON THE STRAIN TRANSFER EFFICIENCY OF AN OPTICAL FIBER SENSOR

Sensor efficiency—effects of materials stiffness				
$T = 400$ μm; $t = 150$ μm; $L = 60$ mm				
Analysis No. (–)	E_{support} (GPa)	E_{coating} (GPa)	E_{adhesive} (GPa)	Δ (%)
1	16.00	3.00	2.50	85.64
2	20.00	3.00	2.50	87.19
3	30.00	3.00	2.50	89.57
4	45.00	3.00	2.50	91.33
5	73.00	3.00	2.50	93.09
6	100.00	3.00	2.50	93.71
7	210.00	3.00	2.50	95.10